Electric conductivity of QCD matter and dilepton spectra in heavy-ion collisions

Ralf Rapp

Cyclotron Institute and Department of Physics and Astronomy, Texas A&M University, College Station, Texas 77843-3366, USA

(Received 4 July 2024; revised 22 August 2024; accepted 22 October 2024; published 20 November 2024)

The electric conductivity, $\sigma_{\rm el}$, is a fundamental transport coefficient of QCD matter that can be related to the zero-energy limit of the electromagnetic (EM) spectral function at vanishing three-momentum in the medium. The EM spectral function is also the central quantity to describe the thermal emission rates and pertinent spectra of photon and dilepton radiation in heavy-ion collisions. Employing a model for dilepton rates that combines hadronic many-body theory with nonperturbative QGP emission constrained by lattice QCD which describes existing dilepton measurements in heavy-ion collisions, I investigate the sensitivity of low-mass dilepton spectra in Pb-Pb collisions at the CERN Large Hadron Collider (LHC) to $\sigma_{\rm el}$. In particular, I separately evaluate the contributions from QGP and hadronic emission, and identify signatures that can help to extract $\sigma_{\rm el}$ from high-precision experimental data expected to be attainable with future detector systems at the LHC.

DOI: 10.1103/PhysRevC.110.054909

I. INTRODUCTION

The hot QCD medium as produced in experiments using ultrarelativistic heavy-ion collisions (URHICs) exhibits remarkable transport properties. Most of the information on those to date has been deduced from phenomenological extractions of the shear viscosity, η, characterizing the transport of energy-momentum, and the charm-diffusion coefficient, $\mathcal{D}_s$, characterizing the transport of the heavy-flavor (HF) quantum number, within the expanding medium. Utilizing relativistic hydrodynamic [1,2] and Brownian motion approaches [3,4] to simulate the momentum spectra of light hadrons and of HF particles, respectively, the dimensionless ratios, $4\pi\eta/s$ (s: entropy density) and $2\pi T\mathcal{D}_s$ (T: temperature), have been estimated to be as small as a factor 2 within lower bounds conjectured for the strong-coupling limit of quantum field theory [5]. Much less is known about the electric conductivity, $\sigma_{\rm el}$, where only recently phenomenological analyses using charge balance function have been conducted, while theoretical calculations in both hadronic and quark-gluon matter [6–11], including lattice-QCD (lQCD) computations [12–14], give rather widely varying results, by over a factor of $\approx$5.

In thermal field theory, transport coefficients can be related to the low-energy limit of the zero-momentum spectral function of the pertinent current of the conserved quantity (e.g., energy-momentum, flavor, or charge). For the electric conductivity this corresponds to the (spatial components of the) electromagnetic (EM) spectral function, $\rho_{\rm em}$. The latter, in turn, is the only spectral function whose medium modifications can be directly measured in nuclear-collision experiments, through the radiation of dileptons which, due to their long mean-free path, can penetrate the strongly interacting system essentially unscathed. Over the past $\approx$ 25 years, a robust understanding has been achieved of the observed low-mass excess of dilepton spectra in heavy-ion collisions over a large range of energies [15,16]. A main conclusion is that the ρ meson, which provides the dominant contribution to hadronic dilepton production, strongly broadens in hadronic matter, with little mass shift, to the extent that the resonance peak "melts" into a quark-antiquark continuum at temperatures near 170 MeV, thereby indicating a transition to partonic degrees of freedom. The EM spectral functions have also been extrapolated to the light cone, i.e., to vanishing invariant mass $M = 0$, to extract thermal photon rates which have been utilized in the interpretation of experimental data for direct-photon production [17–19].

The purpose of the present paper is to carry the in-medium EM spectral functions previously employed in heavy-ion phenomenology to the timelike low-energy limit and (a) extract the pertinent conductivity, and (b) investigate its signatures in dilepton measurements at very low mass and momentum. In this way, I elaborate connections between the microscopic processes that drive the low-mass enhancement of dilepton production in experiment, typically observed in the mass region of a few hundred MeV, and charge transport in the medium.

The remainder of this article is organized as follows. In Sec. II, I recall the basic ingredients to the EM spectral function consisting of in-medium vector-meson spectral functions in hadronic matter and a lQCD constrained rate in the quark-gluon plasma (QGP). In Sec. III, I study the conductivity peak near zero energy, in particular its collisional broadening and the resulting reduction of the conductivity as the zero-energy limit, as well as its manifestation in thermal photon emission rates. In Sec. IV, I investigate the sensitivity of thermal dilepton spectra in Pb-Pb collisions at the CERN Large Hadron

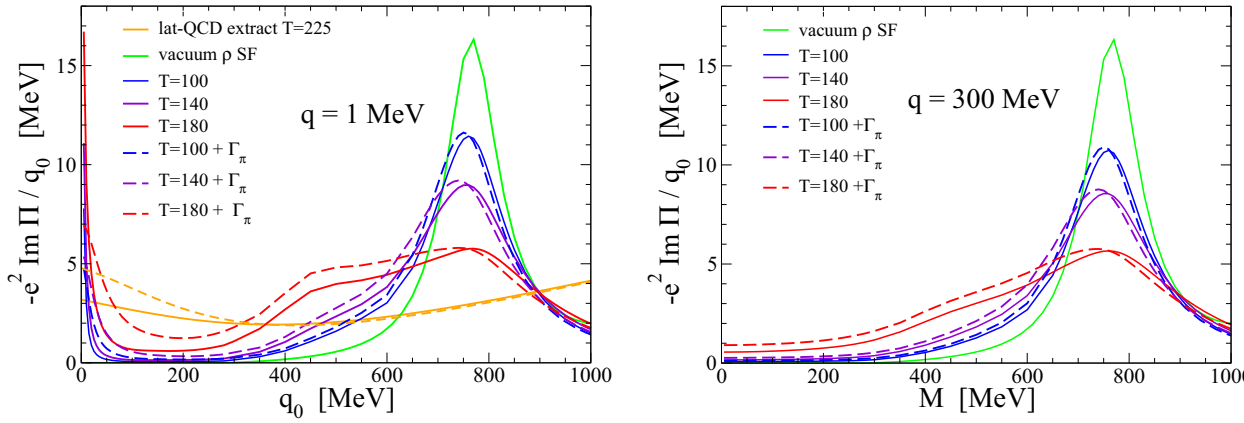

FIG. 1. Electromagnetic spectral functions in hot hadronic matter obtained from in-medium ρ propagators at temperatures (values quoted in units of MeV) and baryon chemical potentials along a thermodynamic trajectory at fixed entropy per baryon, $s/\varrho_B = 330$, and chemical freezeout at $(T, \mu_B) = (160, 22)$ MeV (approximately reflecting the conditions in Au-Au (0.2 TeV) collisions at RHIC). The solid lines are the results based on Ref. [22] while the dashed lines additionally include constant thermal-pion widths based on Ref. [28] ($\Gamma_\pi = 7$–43 MeV for $T = 100$–180 MeV). Left panel: as a function of energy at (near-)vanishing three-momentum, also showing the QGP result at $T \simeq 225$ MeV for the baseline parameters (orange solid line and with a 50% increased conductivity (orange dashed line). Right panel: at a finite three-momentum of $q = 300$ MeV. Note that the spectral functions are divided by energy and multiplied by the electric charge squared so that for vanishing momentum the zero-energy intercept with the abscissa corresponds to the electric conductivity, $\sigma_{\rm el}$.

Collider (LHC) at very low mass ($M \lesssim 0.2$ GeV) to different scenarios of the conductivity in the underlying emission rates; specifically, I show how different acceptance cuts on the single-electron as well as electron pair momenta affect the experimental observables. I summarize and conclude in Sec. V.

II. EM SPECTRAL FUNCTIONS OF QCD MATTER

The thermal rate for dilepton radiation off strongly interacting matter, per unit four-momentum and four-volume, can be expressed via a thermally averaged EM current-current correlation function, $\Pi^{\mu\nu}$, as [20]

$$\frac{dN_{l^+l^-}}{d^4q d^4x} = \frac{\alpha^2 L(M)}{2\pi^3 M^2} f^B(q_0;T)\rho_{\rm em}(M,q;\mu_B,T), \qquad (1)$$

where the EM spectral function, $\rho_{\rm em}$, is related to the imaginary part of the retarded EM current correlator (or in-medium photon self-energy [21]) as $\rho_{\rm em} \equiv -2g_{\mu\nu}\,\mathrm{Im}\,\Pi^{\mu\nu}_{\rm em}/3 = -2\,\mathrm{Im}\,\Pi$ and $\mathrm{Im}\,\Pi = (\mathrm{Im}\,\Pi_L + 2\,\mathrm{Im}\,\Pi_T)/3$. Here, $M^2 = q_0^2 - q^2$ and q denote the invariant-mass squared and three-momentum of the virtual photon, and $L(M)$ is a final-state lepton phase space factor (for either dielectrons or dimuons).

In the following, I recollect the main features of the EM spectral function used in this work, for the case of hadronic matter in Sec. II A and for the QGP in Sec. II B.

A. Hadronic matter: Quantum many-body approach

For the emission rates from hadronic matter, I employ the in-medium vector meson spectral functions developed in Refs. [22–24]. The focus is on the isovector (ρ-meson) channel, which gives the dominant contribution (the contributions of in-medium ω mesons in the isoscalar channel are included in the calculations of dilepton spectra discussed in Sec. IV).

The starting point is an effective, gauge-invariant Lagrangian for $\pi\rho$ interactions in vacuum, whose parameters (bare ρ mass $m_\rho^{(0)}$, $\rho\pi\pi$ coupling constant g_ρ, and a pertinent vertex form factor cutoff Λ_ρ) are fitted to reproduce experimental data for P-wave $\pi\pi$ scattering phase shifts, the pion EM form factor, and the EM spectral function measured in e^+e^- annihilation into hadrons as well as in hadronic τ decays, utilizing the vector dominance model [25–27]:

$$\rho_{\rm em}(M) = -2\frac{\left(m_\rho^{(0)}\right)^4}{g_\rho^2}\,\mathrm{Im}\,D_\rho(M). \qquad (2)$$

Medium effects are calculated based on interactions of the ρ meson and its pion cloud with the surrounding hadronic medium using quantum many-body theory employing effective Lagrangians whose parameters are constrained by empirical decay branchings and scattering data, e.g., resonance decays of mesons (e.g., $a_1 \to \rho\pi$) and baryons ($B^* \to N\rho$) and their radiative decays, photoabsorption on the nucleon and nuclei, and $\pi N \to \rho N$ scattering. As further detailed in Ref. [23], effective baryon densities $\rho_{B,\rm eff}$ in the pion cloud are introduced, defined as the sum of nucleon and antinucleon densities plus half of the densities for excited (anti)baryons. Examples for the in-medium EM spectral functions are shown in Fig. 1, normalized in a way that the zero-energy limit (at vanishing three-momentum) corresponds to the value of the electric conductivity, which will be investigated in more detail in the following section. The spectral functions in hadronic matter, essentially reflecting the in-medium ρ spectral function, exhibit the well-known broadening of the ρ peak as temperature and total baryon density increase, mostly driven by the effects from interactions with baryons and antibaryons [24]. As an improvement over earlier applications to EM observables, necessary to ensure a more reliable evaluation of the very-low-mass region, I have

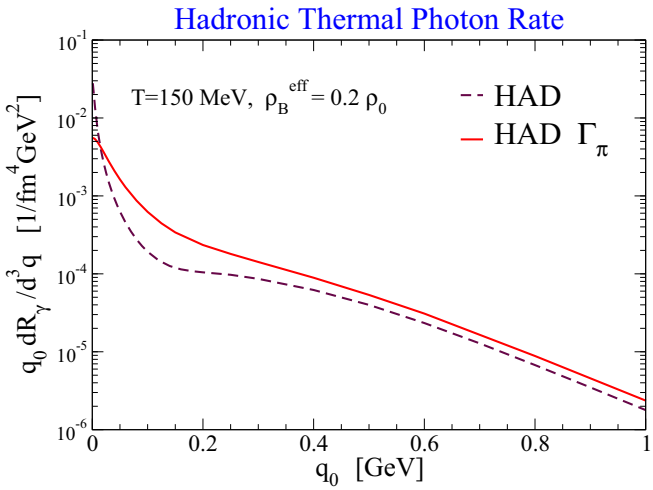

FIG. 2. Thermal hadronic photon rate from the in-medium ρ spectral function with (solid line) and without (dashed line) the contribution from $\pi\pi$ Bremsstrahlung approximated by a thermal-pion induced width in the pion propagators of the ρ-meson self-energy.

replaced the previously used three-level scheme for the pion self-energies from interactions with baryons by a full off-shell treatment (the net effect turns out to be small at higher masses, as will be discussed more quantitatively in the context of dilepton spectra in Sec. IV). In addition, I have augmented the medium modifications of the ρ's pion cloud [22] by accounting for pion widths generated by interactions with thermal pions in the heat bath; these have been estimated from the optical potentials calculated in Refs. [29,30] and implemented as constant values (representing a three-momentum average) amounting to $\approx$43, 26, and 17 MeV at $T = 180$, 140, and 100 MeV, respectively. These effects have long been known to play a rather minor role in the medium modifications of the ρ meson [28], as confirmed here as well (compare the solid vs the dashed lines of the same color).[1] However, they have been found to play a more important role at small energies and specifically for the conductivity in Ref. [29], whose pion gas results are rather accurately reproduced by the pion widths quoted above. As a further illustration of the role of the pion widths generated by interactions with thermal pions (which are mostly mediated through the σ and ρ resonances), Fig. 2 displays the thermal photon rate following from the in-medium ρ spectral function in hadronic matter. The addition of thermal-pion widths has a significant impact on the low-energy rate for energies in the 100–300 MeV region. This is a direct consequence of the broadening of the transport peak, which is accompanied by a quenching of the peak value at $q_0 \to 0$ discernible only at extremely small energies of below $\approx$10 MeV. This suggests that an experimentally measurable signature of a small conductivity is not a peak quenching but rather an enhancement from the peak broadening. The dominant processes underlying the thermal-pion widths are $\pi\pi$ Bremsstrahlung of photons, as can be inferred from pertinent cuts through the imaginary part of the ρ-meson's pion cloud self-energy, with a thermal insertion on both pion lines. The pertinent contribution to photon radiation was investigated previously in Ref. [31] in the context of Super Proton Synchrotron (SPS) direct-photon spectra at very low energies by the WA98 Collaboration [32]. In the calculations of Ref. [31] the Bremsstrahlung's processes have been evaluated explicitly using σ- and ρ-meson pole graphs for the elastic $\pi\pi$ scattering amplitude, and the rate was added incoherently as a separate emission source. Here, the in-medium pion widths subsume these contributions into the ρ self-energy (albeit more schematically from a microscopic point of view); the magnitude and energy dependence of the enhancement in the pertinent photon rate due to the Bremsstrahlung contribution as shown in Fig. 2 are very similar to results in Ref. [31] (see, e.g., the right panel of Fig. 9 there).

B. QGP: Parametrization of lattice-QCD results

For the emission rate from the QGP I employ the construction detailed in Ref. [33], which utilizes a parametrization largely following the lQCD analyses in Refs. [13,34] but with some amendment which I will briefly recall here. It combines a perturbative $q\bar{q}$ annihilation continuum at high masses with a Breit-Wigner peak at low mass, which, in addition, encodes a transition to the high-energy regime at high momentum to resemble the leading-log result for photon production [35]. In this way one can represent and combine the low-energy physics of the conductivity (typically Bremsstrahlung processes, perturbatively of order α_s^2) with photon emission at high energies (typically radiation processes, perturbatively of order α_s) and quark-antiquark annihilation at large invariant mass (which perturbatively is of order 1). No explicit diagrammatic calculation is performed but nonperturbative interaction strength can be captured by constraining the parameters via lQCD data. The pertinent ansatz for the transverse part of the in-medium photon self-energy reads [33]

$$\mathrm{Im}\,\Pi_T = -\frac{N_c C_{\rm em}}{12\pi} M^2 \Big[\hat{f}_2(q_0, q; T) + K F(M^2) 2\pi\alpha_s \frac{T^2}{M^2} \ln\left(1 + \frac{2.912}{4\pi\alpha_s}\frac{q_0}{T}\right)\Big], \quad (3)$$

where $\hat{f}_2$ represents the perturbative $q\bar{q}$ continuum at finite three-momentum [36] (it reduces to $[1 - 2f^F(q_0/2)]$ at vanishing 3-momentum with f^F the Fermi distribution function; strictly speaking, the transverse and longitudinal parts pick up additional pieces at finite three-momentum [37], which, however, do not contribute in the polarization sum needed for calculating dilepton spectra). The second term in the brackets contains a K factor to mimic higher orders in the strong coupling, α_s, and a form factor $F(M^2) = \Lambda^2/(\Lambda^2 + M^2)$ that generates the conductivity peak (with $\Lambda = 2T$ representing its width). I note that at the photon point,

[1] I note that the main medium effect from the surrounding thermal pions on the ρ's pion cloud is caused by the Bose enhancement factors on the pion cloud [30]; this quantum-statistical effect has already been included in Refs. [22,23], corresponding to the solid lines in Fig. 1.

$M = 0$, the second term in brackets generates the leading-log photon rate computed in Ref. [35], which, together with $K = 2$ and $\alpha_s \simeq 0.3$ yields a fairly accurate description [17] of the complete leading-order calculation of Ref. [38]. It also agrees within errors with the recent lQCD computation of the photon rate at $q = 0.8$ GeV [39]: for $N_f = 2$ light flavors it was found that $dN_\gamma/(d^4x d^3q) = \alpha f^B \times (2.2 \pm 0.8) \times 10^{-3}$ GeV, compared to a numerical coefficient of 1.62×10^{-3} GeV resulting from the above baseline parametrization.

Turning to the low-energy limit and $q = 0$, where one can expand the logarithm in q_0/T, one obtains

$$\mathrm{Im}\,\Pi_T^{\mathrm{low}}(q_0, 0) = -\frac{2.912 K N_c C_{\mathrm{em}}}{24\pi} T(2T) \frac{(\Gamma_0/2) q_0}{q_0^2 + (\Gamma_0/2)^2}, \tag{4}$$

where I rewrote the form factor so that the conductivity peak assumes the expected form with a width $\Gamma_0/2 = 2T$. The qualitative features of this expression are (see, e.g., Refs. [13,34,40]) (i) a standard Breit-Wigner representation of the conductivity peak which is norm conserving and has a width $\Gamma_0 \propto T$, (ii) a coefficient representing the quark-number susceptibility that behaves as $\chi_q \propto T^2$, and (iii) a conductivity (defined via the $q_0 \to 0$ limit) that behaves as $\sigma_{\mathrm{el}}/T = \mathrm{const}$ and $\sigma_{\mathrm{el}} \propto 1/\Gamma_0$. Quantitatively, I find that with the parameters chosen in Ref. [33] the static susceptibility turns out to be $\chi_q/T^2 \simeq 0.77$ (for $C_{\mathrm{em}} = 5/9$), which is not far from values extracted from lQCD computations, e.g., 0.88 ± 0.03 at $T = 250$ MeV in Ref. [39]; the constraints on the conductivity will be discussed in more detail in the following section. In what follows below, I will consider an uncertainty estimate where the conductivity is increased by 50%, which also increases the photon rate by the same amount, i.e., the numerical coefficient referred to above increases from 1.62×10^{-3} to 2.43×10^{-3}, being somewhat above the central lQCD value. I caution, however, that the parametrization, Eq. (4), will not work well for small values of the width Γ_0, which produce a large conductivity but also affect the photon rate at high momentum [in this case it is better to use a uniform value of the form-factor parameter Λ in Eq. (3) which will ensure a controlled perturbative limit of the photon rate at high energies]. Pertinent results for the QGP spectral function are shown in the left panel of Fig. 1, exhibiting the 50% increase for $q_0 = 0$. However, the reduced broadening is barely visible as it essentially submerges into the $q\bar{q}$ continuum.

For practical calculations (and to recover the final 1/3 contribution to the conductivity) one also needs to construct a longitudinal part of the photon self-energy, Π_L. This has been done in Ref. [33] using guidance from current conservation and in analogy to the Lagrangians used for ρ-baryon S-wave interactions in hadronic matter (see, e.g., Ref. [27]), with the ansatz $\Pi_L = M^2/q_0^2\ \Pi_T$ for the nonperturbative (second) term in Eq. (3). This is clearly a rather schematic ansatz that should be checked more quantitatively in the future against lQCD data at finite three-momentum, such as those in Ref. [39]. Unless otherwise stated, the calculations below are performed for the three-flavor case with $C_{\mathrm{em}} = 6/9$.

III. CONDUCTIVITY

Let me now turn to the conductivity by exploiting its definition as the (timelike) zero-energy limit of the EM spectral function at vanishing three-momentum,

$$\sigma_{\mathrm{el}}(T) = \frac{e^2}{2} \lim_{q_0 \to 0} \rho_{\mathrm{em}}(q_0, q = 0)/q_0\ . \tag{5}$$

In the previous section I have already alluded to the importance of the pion cloud contributions to the low-energy part of the hadronic EM spectral function. It turns out that the direct ρ-meson interactions with mesons and baryons from the heat bath, which are implemented via resonance interactions [e.g., $\rho + \pi \to a_1$ or $\rho + N \to N^*(1520)$, respectively], result in ρ-meson self-energies that do not contribute to the conductivity. The reason for that is that the underlying interaction Lagrangians for the three-point vertices need to satisfy current conservation, which is achieved by using couplings to the ρ-meson field strength tensor, $\rho^{\mu\nu}$. The derivatives in this coupling result in self-energies which are proportional to the square of the ρ's energy, three-momentum, or invariant mass [27]. In any case, it entails a vanishing contribution to the conductivity (this was also found for the charge susceptibility χ_{ch}, which can be extracted from the spacelike limit of the EM spectral function, ρ_{em} $(q_0 = 0, q \to 0)$ [41]).

Therefore, I focus on the pion cloud contributions to the ρ self-energy in this section. The low-energy region of the EM spectral functions, shown in Fig. 3 left, exhibits rather large values of $\sigma_{\mathrm{el}} \simeq 20$–$40$ MeV when only baryonic resonance excitations of the pions are included (currently limited to P-wave excitations $\pi + B_1 \to B_2$). However, the inclusion of a constant pion width estimated from interactions with thermal pions markedly reduces the conductivity by a factor of 4–5 down to values of $\sigma_{\mathrm{el}} \approx 5$–$7.5$ MeV, in line with the recent microscopic calculations in Ref. [29]. At the same time the medium modifications in the ρ-resonance peak region due to thermal pion widths are much less pronounced (see right panel of Fig. 3). Also recall that the total pion cloud modification in the low-mass region, which is mostly due to the effects from baryons, makes up a $\approx 1/3$ portion of the total ρ broadening when also the direct ρ-hadron interactions are accounted for (see left panel of Fig. 1). This suggests that the conductivity chiefly probes medium effects due to the light charge carriers in the hadronic medium, while the ρ melting at higher masses is mostly driven by rescattering of the pions and ρ mesons on the (anti)baryons in the medium.

For the QGP spectral function, the parametrization detailed in the previous section, with the baseline parameters from Ref. [33], yields $\sigma_{\mathrm{el}}/T \simeq e^2 0.23 C_{\mathrm{em}}$, which, using $C_{\mathrm{em}} = 6/9$, evaluates to 0.014, quite compatible with recent lQCD computations for temperatures $T \gtrsim 200$ MeV, as reported in Refs. [12–14,42] (note that in these works, the factor $e^2 C_{\mathrm{em}}$ is usually taken out, which for my results corresponds to 0.23); cf. also Ref. [43]. The ρ spectral functions based on Refs. [22,23] lead to much larger conductivities, $\sigma_{\mathrm{el}}/T \simeq 0.2$, with a rather weak temperature dependence. When including the dressing of the ρ's pion cloud via interactions with thermal

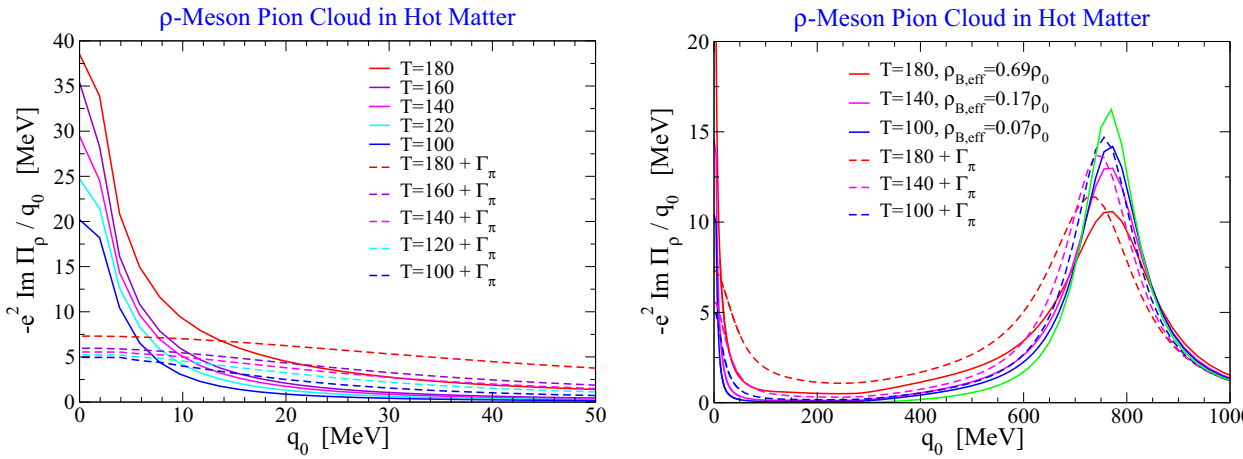

FIG. 3. Hadronic EM spectral function in the isovector channel at total three-momentum $q = 1$ MeV as obtained when only modifications of the ρ-meson's pion cloud are accounted for (left panel: very-low-mass region including the conductivity peak at vanishing energy; right panel: across the ρ-meson resonance region). Solid lines correspond to the full off-shell calculations when only including the medium modifications induced by (anti)baryons (plus Bose enhancement factors for the intermediate pions), while the solid lines additionally include thermal pion widths extracted from microscopic calculations using realistic $\pi\pi$ interactions. All temperatures are quoted in units of MeV.

pions, this value drops to ≈0.04, which is much closer to the lQCD result (albeit still significantly larger). However, in the vicinity of the pseudocritical region, lQCD computations lead to even smaller values, $\sigma_{\rm el}/T \simeq C_{\rm em}e^2 0.05 \simeq 0.003$, with relative large systematic errors. At face value, these results are smaller than quantum lower bounds estimated from the AdS/CFT correspondence. The origin of the large discrepancy between the lQCD results and hadronic calculations in the pseudocritical region deserves further study. In the present context, I retain my more schematic model for the QGP emission where the difference between the QGP and hadronic results is much smaller. Possible additional contributions in the hadronic calculations might arise from pion interactions with thermal kaons (which are typically at a level of 20% of the pion contributions), S-wave pion-baryon interactions (which are usually much weaker than the P-wave ones [44]), or gauge-invariant coupling schemes for direct ρ-hadron interactions that are not based on the ρ-meson field-strength tensor. To give an indication of the uncertainty in my QGP calculations of the EM spectral function, especially concerning the very-low mass region in connection with the conductivity, I will also conduct dilepton calculations where the width of the low-mass peak is reduced by a factor of 2 by using $\Gamma_0 = 2T$. This will *increase* the conductivity by a factor of 2, to about $\sigma_{\rm el}/T = 0.028$, which reduces the gap to the hadronic calculation (in principle, one would like to have a continuous transition). Note, however, that the accompanying narrowing of the peak in principle suppresses its tail into the low-mass region (although ths is not very apparent due to the large QGP width, Γ_0). This feature (also related to a sum rule) is not always implemented in existing calculations in the literature, where sometimes an ansatz for the photon rate has been made that is directly proportional to $\sigma_{\rm el}$ [45,46]. Without the energy dependence from the Lorentzian peak this leads to an energy-independent increase of the rate with increasing $\sigma_{\rm el}$.

IV. DILEPTON SPECTRA

Next, I proceed to compute dilepton spectra in heavy-ion collisions at the LHC using thermal emission rates based on the spectral functions discussed in the preceding section (in addition to the in-medium ρ I also include the isoscalar contribution from in-medium ω mesons and a multimeson continuum at invariant masses above ≈1 GeV; both contributions are, however, immaterial for the purpose of the present discussion). Following earlier applications, I employ a schematic cylindrical fireball model assuming an isotropic medium with isentropic expansion over which the rates are convoluted to obtain the spectra,

$$\frac{dN_{l^+l^-}}{dM} = \int \frac{M d^3q}{q_0} d\tau\, V_{\rm FB}(\tau) \frac{dN_{l^+l^-}}{d^4q d^4x} \,. \tag{6}$$

The expansion parameters (relativistic transverse and longitudinal accelerations and speeds) and total entropy, $S_{\rm tot}$, in the fireball volume, $V_{\rm FB}(t)$, are adjusted to reproduce blast-wave results for the kinetic freezeout of light-hadron spectra as well as their experimentally observed multiplicities for a given centrality class, respectively. To convert the thus obtained time-dependent entropy density $s(T) = S_{\rm tot}/V_{\rm FB}$ into a temperature requires the equation of state of the system; a parametrization of lQCD data above $T = 170$ MeV, smoothly matched to a hadron resonance gas below, was used. Hadrochemical freezeout is implemented at $(\mu_B, T_{\rm chem}) \simeq (1, 160)$ MeV, after which effective chemical potentials are introduced for the light hadrons which are stable under strong decays (including anti-baryons) to keep their ratios constant throughout the hadronic evolution. Kinetic freezeout typically occurs around $T_{\rm kin} = 100$ MeV in central Pb-Pb collisions at the LHC. Note that more sophisticated space-time evolutions in terms of viscous hydrodynamics [47] or coarse-graining of transport simulations [48] have been applied to compute dilepton production at collider energies. These calculations usually

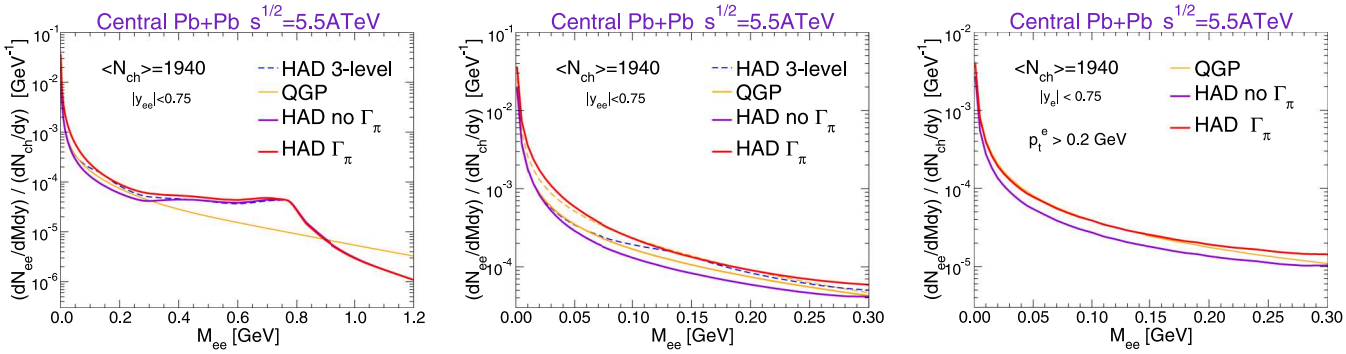

FIG. 4. Three-momentum integrated low-mass dilepton spectra from thermal radiation in central Pb-Pb (5.02 TeV) collisions, with only an acceptance cut on the pair rapidity applied; the left (middle) panel shows the (very-)low-mass region, while the right panel includes an extra cut on the single-electron p_t. The dotted line is the result for the previously used three-level approximation for the baryon-induced medium modifications in the pion cloud of the ρ meson, while the solid red and purple lines are using a full off-shell integration over the pion self-energy with and without the addition of a pion width from interactions with pions in the heat bath, respectively; the orange solid line represents the baseline QGP contribution while the dashed orange line in the middle panel correspond to an increase in the conductivity by 50%.

achieve a similar degree of agreement with experimental data compared to the schematic fireball expansion utilized here, and thus the latter may still serve as a fair means to predict features of thermal radiation in future data in the (very-)low-mass region.

While the dilepton mass spectrum is in principle Lorentz invariant, experimental acceptance cuts on the leptons generally spoil this property. In practice, Eq. (6) is evaluated in the local rest frame of the fireball, the virtual photon is decayed into leptons, and their four-momenta are then boosted into the laboratory frame and subjected to experimental cuts. I first inspect the three-momentum integrated dielectron invariant-mass spectra (setting the electron mass to zero) with minimal restrictions on the measured kinematics of the lepton pair applied, i.e., merely a pair-rapidity cut around midrapidity of $|y_{ee}| < 0.75$. From the left panel of Fig. 4 one sees the usual feature that hadronic emission dominates in the ρ resonance region with a strongly smeared-out peak, while QGP emission at the LHC takes over for invariant masses $M \gtrsim 1$ GeV. At very low masses, i.e., below the two-pion threshold, $M \lesssim 300$ MeV, both contributions are comparable. Finer details can be seen when zooming in to this region; cf. middle panel of Fig. 4. Within the previously employed three-level approximation for the baryon-induced self-energies of the pions, hadronic emission is slightly larger than the baseline for QGP radiation, by up to ≈20% or so, around $M \simeq 150$ MeV (note that above the two-pion threshold there is little difference between the full calculation and the three-level approximation). However, with the more accurate full off-shell calculations [22], the hadronic emission is mostly below the QGP emission by up to 20% or so. Finally, when including additional pion widths estimated from interactions with the surrounding pion gas, one is back to a situation where hadronic emission is slightly stronger, with the enhancement now growing toward smaller masses, amounting, e.g., to ≈50% at $M = 50$ MeV. Recalling that the conductivity is much smaller for the case with thermally induced pion widths, one can conclude that dileptons at very low masses are indeed quite sensitive to the electric conductivity: a factor of about 5 *reduction* in the conductivity leads to an *enhancement* of more than a factor of 2 in the three-momentum integrated dilepton spectrum at $M = 50$ MeV (for the hadronic contribution). This implies that, much like for the photon rates, the observable effect of changes in the conductivity is the broadening of the conductivity peak, not its reduction at the zero-energy intercept. On the other hand, the situation for QGP emission seems to be the opposite, i.e., an *increase* in the conductivity also leads to an increase in the very-low-mass dilepton yield. This is due to the much larger broadening of the conductivity peak in the QGP to begin with, so that an enhancement of the peak region can still *increase* the dilepton yields in the mass region up to ≈300 MeV. Finally, when applying a rather common experimental acceptance cut where the transverse momentum of the individual electron and positron tracks is restricted to $p_t^e > 0.2$ GeV, the sensitivity to the hadronic conductivity reduces appreciably, i.e., the enhancement at $M = 50$ MeV is only at a level of ≈50%, while an increased QGP conductivity (not shown) still enhances the pertinent emission over the baseline scenario at larger masses (e.g., by 20–25% at $M = 200$ MeV).

Recalling the EM spectral functions in Fig. 1, which indicate that the conductivity peak has essentially disappeared for a three-momentum of $q = 300$ MeV (note that at this momentum, $M = 0$ corresponds to a photon energy of 300 MeV), I investigate the impact of an upper cut on the electron pair's (or virtual photon's) transverse momentum, q_t^{ee}, in Fig. 5. Note that this differs from the three-momentum, q, of the EM spectral function in the thermal rest frame by a Lorentz-boost caused by the collective expansion of the fireball medium. Nevertheless, when $q_t^{ee} < 0.2$ GeV is imposed, the enhancement from the hadronic scenario with smaller conductivity (due to the thermal pion widths) over QGP emission increases, to a factor of 3 at $M = 50$ MeV (compared to 2 without the cut); see left panel in Fig. 5. At the same time, the enhancement of the QGP rate with larger conductivity remains at 20% over the baseline scenario (very similar to the case without the pair-q_t cut). With a more extreme choice of $q_t^{ee} < 0.03$ GeV, the enhancement of the hadronic rate rises further, to almost a factor of 4. There is, of course, a price to pay in that the pertinent yields in the spectra are substantiality

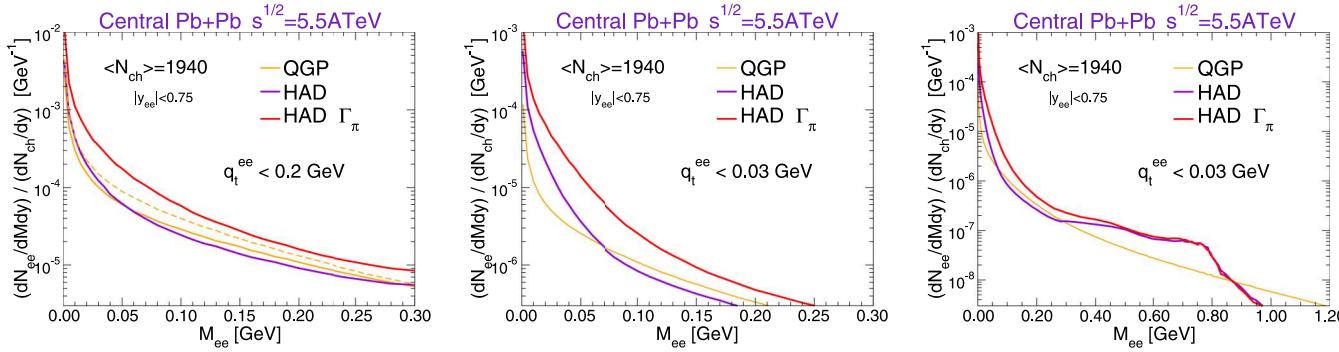

FIG. 5. Very low-mass dilepton spectra in central Pb-Pb collisions at the LHC when applying an upper limit on the pair momentum of $q_t^{ee} < 0.2$ GeV (left panel) and 0.03 GeV (middle panel); note the reduction in the overall yield for the latter case, which is also shown over a wider mass region in the right panel, relative to the left panel in Fig. 4. Same line identifications as in Fig. 4.

suppressed, by a factor of ≈ 3 for $q_t^{ee} < 0.2$ GeV and about an additional order of magnitude for $q_t^{ee} < 0.03$ GeV. An optimized experimental sensitivity will thus have to balance an enhancement due to the reduced conductivity with the loss of total yield.

V. CONCLUSIONS

In this paper I studied the electric conductivity of hot QCD matter and its manifestation in thermal dilepton spectra in ultarelativistic heavy-ion collisions, utilizing their formal connection through the EM spectral function. In the hadronic phase, I employed in-medium vector-meson spectral functions computed in hadronic many-body theory in connection with the vector dominance model to couple to the EM current; in particular, I improved the calculation of the in-medium pion cloud of the ρ-meson's self-energy through an explicit off-shell treatment which turned out to be quantitatively important for the very-low mass region of the EM spectral function. Furthermore, the addition of thermal pion widths was found to produce the most relevant contribution to broadening the conductivity peak near zero energy. This, in particular, suggests that the light degrees of freedom in hadronic matter are the key carriers of the EM current, while in the ρ resonance region baryon-induced effects are dominant. For the quark-gluon plasma, I used a perturbative $q\bar{q}$ spectrum augmented with a conductivity peak that matches lattice QCD data at temperatures above $\approx$200 MeV. At lower temperatures the lattice data show a rather strong decrease in $\sigma_{\rm el}/T$ that leads to a marked discrepancy with the hadronic calculations which requires further study (e.g., by scrutinizing the in-medium selfenergies of the pions). When applying this setup to compute thermal dilepton spectra I found that the chief signature of a small conductivity in hadronic matter is an enhancement in the dilepton yields in the mass region below the two-pion threshold, caused by the broadening of the conductivity peak at zero energy. Since the latter rapidly ceases at finite three-momentum, the signal can be enhanced by applying upper cuts on the lepton pair momentum, while in practice this will have to be balanced by the accompanying strong reduction in the total yields. On the other hand, for a very large broadening of several hundred MeV, as current lQCD calculations suggest for the QGP phase, an increase of the conductivity can also lead to a modest increase over an appreciable range in the dilepton yield for masses up to 300 MeV or so. Overall, the sensitivity of the very-low-mass region in thermal dilepton radiation is promising for a meaningful measurement with future precision data at ALICE-3 in run 5 at the LHC. In the meantime, efforts are underway to improve the theoretical knowledge about the magnitude of the conductivity in the pseudocritical region.

ACKNOWLEDGMENTS

This work was supported by U.S. National Science Foundation through Grant No. PHY-2209335. The author gratefully acknowledges Michael Urban for providing his code for the off-shell calculations of the in-medium pion cloud of the ρ meson.

[1] U. Heinz and R. Snellings, Annu. Rev. Nucl. Part. Sci. **63**, 123 (2013).
[2] H. Niemi, K. J. Eskola, and R. Paatelainen, Phys. Rev. C **93**, 024907 (2016).
[3] A. Beraudo *et al.*, Nucl. Phys. A **979**, 21 (2018).
[4] X. Dong, Y.-J. Lee, and R. Rapp, Annu. Rev. Nucl. Part. Sci. **69**, 417 (2019).
[5] G. Policastro, D. T. Son, and A. O. Starinets, J. High Energy Phys. 09 (2002) 043.
[6] D. Fernandez-Fraile and A. Gomez Nicola, Eur. Phys. J. C **62**, 37 (2009).
[7] R. Marty, E. Bratkovskaya, W. Cassing, J. Aichelin, and H. Berrehrah, Phys. Rev. C **88**, 045204 (2013).
[8] C.-H. Lee and I. Zahed, Phys. Rev. C **90**, 025204 (2014).
[9] M. Greif, I. Bouras, C. Greiner, and Z. Xu, Phys. Rev. D **90**, 094014 (2014).
[10] M. Greif, C. Greiner, and G. S. Denicol, Phys. Rev. D **93**, 096012 (2016); **96**, 059902(E) (2017).

[11] S. Ghosh, Phys. Rev. D **95**, 036018 (2017).
[12] G. Aarts, C. Allton, A. Amato, P. Giudice, S. Hands, and J.-I. Skullerud, J. High Energy Phys. 02 (2015) 186.
[13] B. B. Brandt, A. Francis, B. Jäger, and H. B. Meyer, Phys. Rev. D **93**, 054510 (2016).
[14] H.-T. Ding, O. Kaczmarek, and F. Meyer, Phys. Rev. D **94**, 034504 (2016).
[15] R. Rapp, J. Wambach, and H. van Hees, Landolt-Bornstein **23**, 134 (2010).
[16] R. Rapp and H. van Hees, Eur. Phys. J. A **52**, 257 (2016).
[17] S. Turbide, R. Rapp, and C. Gale, Phys. Rev. C **69**, 014903 (2004).
[18] H. van Hees, M. He, and R. Rapp, Nucl. Phys. A **933**, 256 (2015).
[19] J.-F. Paquet, C. Shen, G. S. Denicol, M. Luzum, B. Schenke, S. Jeon, and C. Gale, Phys. Rev. C **93**, 044906 (2016).
[20] E. L. Feinberg, Nuovo Cim. A **34**, 391 (1976).
[21] H. A. Weldon, Phys. Rev. D **42**, 2384 (1990).
[22] M. Urban, M. Buballa, R. Rapp, and J. Wambach, Nucl. Phys. A **673**, 357 (2000).
[23] R. Rapp and J. Wambach, Eur. Phys. J. A **6**, 415 (1999).
[24] R. Rapp, Phys. Rev. C **63**, 054907 (2001).
[25] N. M. Kroll, T. D. Lee, and B. Zumino, Phys. Rev. **157**, 1376 (1967).
[26] C. Gale and J. I. Kapusta, Nucl. Phys. B **357**, 65 (1991).
[27] R. Rapp and J. Wambach, Adv. Nucl. Phys. **25**, 1 (2000).
[28] R. Rapp and J. Wambach, Phys. Lett. B **351**, 50 (1995).
[29] J. Atchison and R. Rapp, Nucl. Phys. A **1037**, 122704 (2023).
[30] R. Rapp and J. Wambach, Phys. Lett. B **315**, 220 (1993).
[31] W. Liu and R. Rapp, Nucl. Phys. A **796**, 101 (2007).
[32] M. M. Aggarwal *et al.* (WA98 Collaboration), Phys. Rev. Lett. **93**, 022301 (2004).
[33] R. Rapp, Adv. High Energy Phys. **2013**, 148253 (2013).
[34] H. T. Ding, A. Francis, O. Kaczmarek, F. Karsch, E. Laermann, and W. Soeldner, Phys. Rev. D **83**, 034504 (2011).
[35] J. I. Kapusta, P. Lichard, and D. Seibert, Phys. Rev. D **44**, 2774 (1991); **47**, 4171(E) (1993).
[36] J. Cleymans, J. Fingberg, and K. Redlich, Phys. Rev. D **35**, 2153 (1987).
[37] G. Aarts and J. M. Martinez Resco, Nucl. Phys. B **726**, 93 (2005).
[38] P. B. Arnold, G. D. Moore, and L. G. Yaffe, J. High Energy Phys. 12 (2001) 009.
[39] M. Cè, T. Harris, A. Krasniqi, H. B. Meyer, and C. Török, Phys. Rev. D **106**, 054501 (2022).
[40] G. D. Moore and J.-M. Robert, arXiv:hep-ph/0607172.
[41] M. Prakash, R. Rapp, J. Wambach, and I. Zahed, Phys. Rev. C **65**, 034906 (2002).
[42] N. Astrakhantsev, V. V. Braguta, M. D'Elia, A. Y. Kotov, A. A. Nikolaev, and F. Sanfilippo, Phys. Rev. D **102**, 054516 (2020).
[43] G. Aarts and A. Nikolaev, Eur. Phys. J. A **57**, 118 (2021).
[44] N. P. M. Holt and R. Rapp, Eur. Phys. J. A **56**, 292 (2020).
[45] D. Fernandez-Fraile and A. Gomez Nicola, Phys. Rev. D **73**, 045025 (2006).
[46] S. Floerchinger, C. Gebhardt, and K. Reygers, Phys. Lett. B **837**, 137647 (2023).
[47] G. Vujanovic, C. Young, B. Schenke, R. Rapp, S. Jeon, and C. Gale, Phys. Rev. C **89**, 034904 (2014).
[48] S. Endres, H. van Hees, and M. Bleicher, Phys. Rev. C **94**, 024912 (2016).